Acta Pharmaceutica Sinica B 2026;16(6):3729−3745

Chinese Pharmaceutical Association
Institute of Materia Medica, Chinese Academy of Medical Sciences

Acta Pharmaceutica Sinica B

www.elsevier.com/locate/apsb
www.sciencedirect.com

ORIGINAL ARTICLE

NFYB−lncRNA axis resets the tumor microenvironment to promote HCC aggressive progression by a positive feedback loop

Boxuan Zhou[a,b,†], Qiang Tao[c,†], Wu Wen[d,†], Jianan Tan[b,e,†], Jie Xu[f], Yixuan Fang[g], Jiao Guan[b,h], Xiaorong Lin[i], Jiehua He[b,h], Milad Ashrafizadeh[j], Zifeng Wang[k,*], João Conde[l,*], Fang Zheng[b,h,*]

[a]*Department of Breast Disease Center, General Surgery, The First Affiliated Hospital, Jiangxi Medical College, Nanchang University, Nanchang 330006, China*
[b]*Guangdong Provincial Key Laboratory of Malignant Tumor Epigenetics and Gene Regulation, Sun Yat-sen Memorial Hospital, Sun Yat-sen University, Guangzhou 510120, China*
[c]*Department of Hepatobiliary and Pancreatic Surgery, The Eighth Affiliated Hospital, Sun Yat-sen University, Shenzhen 518033, China*
[d]*Department of Hepatobiliary and Pancreatic Surgery, General Surgery, The First Affiliated Hospital, Jiangxi Medical College, Nanchang University, Nanchang 330006, China*
[e]*Department of Gastrointestinal Surgery, The Affiliated Guangdong Second Provincial General Hospital of Jinan University, Guangzhou 510317, China*
[f]*Department of Pathology, Guangdong Provincial People's Hospital, Guangzhou 510060, China*
[g]*International Department, Affiliated High School of South China Normal University, Guangzhou 510620, China*
[h]*Medical Research Center, Sun Yat-sen Memorial Hospital, Sun Yat-sen University, Guangzhou 510120, China*
[i]*Diagnosis and Treatment Center of Breast Diseases, Shantou Central Hospital, Shantou 515031, China*
[j]*Department of Radiation Oncology, Shandong Provincial Key Laboratory of Radiation Oncology, Shandong Cancer Hospital and Institute, Shandong First Medical University, Shandong Academy of Medical Sciences, Jinan 250000, China*
[k]*State Key Laboratory of Oncology in South China, Sun Yat-sen University Cancer Center, Collaborative Innovation Center for Cancer Medicine, Guangzhou 510060, China*
[l]*Comprehensive Health Research Centre, NOVA Medical School, Faculdade de Ciências Médicas, Universidade NOVA de Lisboa, Lisboa 1169-056, Portugal*

Received 23 June 2025; received in revised form 11 November 2025; accepted 15 December 2025

*Corresponding authors.
E-mail addresses: zhengf9@mail.sysu.edu.cn (Fang Zheng), joao.conde@nms.unl.pt (João Conde), wangzf@sysucc.org.cn (Zifeng Wang).
[†]These authors made equal contributions to this work.
Peer review under the responsibility of Chinese Pharmaceutical Association and Institute of Materia Medica, Chinese Academy of Medical Sciences.

https://doi.org/10.1016/j.apsb.2026.03.037

KEY WORDS

HCC;
NF-Y family;
lncRNA;
Tumor microenvironment;
Macrophage;
Cytokines secretion;
Metastasis;
Combined treatment

Abstract Metastases are a primary cause of cancer-associated mortality; however, the mechanisms underlying aggressive progression have not been clearly elucidated. Genome-wide features of chromatin accessibility through ATAC-seq from HCC primary and metastatic tumors revealed that many distal regulatory elements spreading the genome become accessible during aggressive progression, the changes of which are associated with NFY-family. And NFYB is frequently upregulated in tumor with metastasis. Mechanistically, LINC01137 recruits SMYD3 to enhance H3K4me3 occupancy at IL-1β, CXCL2 and CCL20 promoters by inhibiting lysine ubiquitination to stabilize NFYB, which in turn upregulates IL-1β, CXCL2 and CCL20. HCC-derived cytokine transforms macrophages to the M2 phenotype to foster an inhibitory tumor microenvironment and anti-PDL1 tolerance. Importantly, LINC01137 transcription is activated by the NFYB/KAT2B complex in a feed-forward loop. Notably, treatment with an IL-1β inhibitor enhances the blockade efficacy of PD-L1 in NFYB-overexpressing HCC. Our findings imply an immunosuppressive role of NFYB−LINC01137 signaling during aggressive HCC progression and support the concept of microenvironment engineering in immunotherapy.

1. Introduction

Hepatocellular carcinoma (HCC) is the most aggressive human malignancies globally, which is ranked as the third leading cause of cancer-related death[1]. Compelling evidence indicates that poor clinical outcomes of HCC are largely ascribed to the high incidences of intrahepatic and extrahepatic metastases[2]. As such, it is imperative to explore the mechanisms underlying HCC metastasis to lay the foundation for developing new therapeutic targets for successful intervention.

It has been established that the tumor microenvironment of HCC is characterized by infiltrations of immunosuppressive cells, including tumor-associated macrophages (TAMs) which are phenotypically and functionally similar to alternately activated (M2-like) macrophages, and activation of immune checkpoint signals[3]. As the representative immunosuppressive population in HCC, TAMs accelerate tumor aggressive progression, inhibit anti-tumor immune response by expressing series of effector molecules containing cytokines, chemokines, enzymes and cell surface receptors[4]. And it is imperative to explore the tumor-intrinsic oncogenic signaling that drives the accumulation of TAMs and the underlying molecular mechanisms in human HCC, and reversing the M2 phenotype, blocking the TAMs recruitment and preventing TAMs infiltration are expected to be effective strategies for HCC therapy.

It has been documented that NF-Y is a highly conserved and ubiquitously expressed heterotrimeric transcriptional activator composed of NF-YA, NF-YB, and NF-YC subunits[5]. The interaction of NF-YB/NF-YC with NF-YA confers the NF-Y complex with sequence-specific targeting capability and nucleosome-like properties of non-specific DNA binding through the non-specific histone-fold domain (HFD) DNA contacts, a combination that ensures stable DNA binding[6,7]. The binding of NF-Y to DNA mediates histone posttranslational epigenetic modifications (PTMs) on active promoters by recruiting relevant enzymes, allowing for complex NF-Y biology, for example, by acting as a key regulator of cell-cycle progression in proliferating cells[8-10]. And a recent study showed that NFYB increases chemosensitivity in glioblastoma by promoting HDAC5-mediated transcriptional inhibition of *SHMT2*[11]. Zhao et al.[12] also reported that NFYB potentiates STK33 activation to promote cisplatin resistance in diffuse large B-cell lymphoma. In addition to binding core promoters, intriguing evidence shows that NF-Y can bind to enhancer elements away from transcription start sites thereby promoting chromatin accessibility in the maintenance of ESC identity[7]. And NFYB which regulated mitochondrial function and longevity *via* lysosomal prosaposin has been reported to be upregulated in esophageal cancer, gastric cancer and all stages of HCC, and its expression level was correlated with the poor survival of patients[13-15]. Wang et al.[16] also displayed that coptisine-mediated downregulation of *E2F7* induces G2/M phase arrest through inhibition of E2F4/NFYA/NFYB transcription factors in hepatocellular carcinoma cells. These results indicate that NFYB plays the important role in HCC, and identifying other functions and mechanism of NFYB will provide much better acknowledge of HCC aggressive progression.

Long non-coding RNAs (lncRNAs), a large class of non-protein-coding RNA transcripts, exert crucial functions in numerous physiological and pathological processes through epigenetic regulation and related signal transduction[17,18]. Recently published data suggest that lncRNAs may play key regulatory roles in cellular signal transduction pathways by interacting with major signaling proteins[19,20]. In this study, the mechanisms that drive HCC metastatic progression are investigated using pure cancer cell populations isolated from both primary tumors and metastases from HCC patients.

2. Materials and methods

2.1. Tissue specimens

See Supporting Information 'Materials and methods' for details.

According to the protocol approved by the institutional review board, HCC and adjacent normal tissue samples were obtained with informed consent. These samples were collected at the Cancer Center, Sun Yat-sen University and Guangdong Provincial People's Hospital (Guangzhou, China) between July 2009 and June 2019. All samples were collected with signed informed consent from patients and Ethics approval number: (2024) CDYFYYLK (05-008). The selection of HCC cases was based on a clear pathological diagnosis, follow-up data, and the selected cases had not received previous local or systemic treatment.

Tumor stage was defined according to the 2002 American Joint Committee on Cancer/International Union Against Cancer tumour-node-metastasis classification system. This study was approved by ethics *committee* of the First Affiliated Hospital, Jiangxi Medical College, Nanchang University.

2.2. *ATAC-seq library preparation and differential accessibility*

ATAC-seq data were analyzed according to guidelines of Harvard FAS Informatics (https://informatics.fas.harvard.edu/atac-seq-guidelines.html). Optimally, reads were aligned to the reference human genome (GRCh37/hg19) using HISAT2 with X, no-spliced-alignment, and no-temp-splice site parameters following the manual to replace bowtie2. PCR duplicates were removed using Picard MarkDuplicates. Peaks were annotated by mapping to the nearest TSS using the Homer annotate Peaks tool. Overlapped unique peaks were identified by using BEDtools. Further, transcription factor footprints (TFF) were identified by the HINT tool from the Regulator Genomics Toolbox (RGT, https://www.regulatory-genomics.org/hint/method/) in significant peaks on all samples separately.

2.3. *RNA-sequencing expression analysis*

RNA-sequencing (RNA-seq) libraries were prepared using the Illumina TruSeq Kit (v.2), according to the manufacturer's instructions. RNA-seq reads were separately aligned to the mouse genome (mm10) using TopHat. Read counts within merged exons (RefSeq) were found and compared using DESeq2[21]. The coverage track (bigWig) files of RNA-seq data were generated using BAM file and normalized by bins per million mapped reads (BPM, same as TPM).

2.4. *In vivo metastasis assays and orthotopic HCC mouse model*

In vivo metastasis assays and orthotopic HCC mouse model were established as described in Supporting Information materials and methods.

2.5. *Statistics analysis*

All statistical analyses were performed using SPSS 16.0 statistical software package and Graphpad Prism 8. For most of the *in vitro* and animal experiments, unpaired two-sided Student's *t* test and one-way ANOVA was used to calculate the *P* value, and *post hoc* tests were used to test the difference between groups. Chi-square test was used to analyze the relationship between LINC01137 expression and clinicopathological status.

3. Results

3.1. *Two distinct chromatin accessibility landscapes in primary and metastatic HCC*

To explore genome-wide chromatin accessibility landscape in primary and metastatic HCC, primary tumor (primary) and corresponding lung metastases (metastasis) cells were isolated from two patients and cultured, which was followed by an assay of transposase-accessible chromatin through sequencing (ATAC). Differential accessibility between the two groups showed that 29.8% of all accessible regions were unique to the predominantly metastatic group. Contrarily, 35.9% of peaks were specific to the primary-tumor-enriched group (Fig. 1A and B). Furthermore, GREAT analysis was performed to explore the distribution and potential biological functions of the top 2000 dynamic accessible chromatin regions. Analysis suggested that a majority of dynamic differentially accessible chromatin regions were gene-distal, with relatively few promoter-proximal regions depicting differential accessibility (Fig. 1C). Gene ontology (GO) analysis revealed that metastatic-specific accessible chromatin regions were enriched for genes associated with immune system, cell cytokine and chemokine production, while the primary tumor-specific accessible chromatin regions were relevant to cell migration and immune response (Fig. 1D). These results provide evidence that primary and metastatic tumors are related to the tumor immune microenvironment (TIME).

3.2. *NFYB is a crucial gene associated with immunosuppression and unfavorable prognosis in patients with HCC*

To identify potential drivers of this difference in accessibility, transcription factor motif enrichment within the differentially accessible regions was performed with the HINT-ATAC software[22]. Several TFs with significantly different binding activities between primary and metastatic tumors were identified as candidates for precise foot-printing analysis (Fig. 1E). This analysis demonstrated that the binding activities of chromatin architectural transcription factors in the NF-Y family were significantly increased in metastatic tumor samples, with NFYB exhibiting a much higher activity than NFYA (Fig. 1F and Supporting Information Fig. S1A). Analysis of the protein levels in two paired primary and metastatic tumors showed that NFYB expression was significantly upregulated in metastatic tumors, NFYA expression was only slightly elevated while the differences in the NFYC subunit were not significant (Fig. S1B). Consistently, the high metastatic HCC cell line, HCCLM9 and MHCC97H, had the highest levels of NFYB (Fig. 1G). Furthermore, NFYB was significantly increased in samples with metastasis by IF, compared to those without metastasis (Fig. 1H). And the above results were confirmed by IHC in 149 HCC samples (Fig. 1I and J). Correlation analysis showed that elevated NFYB in HCCs was significantly associated with a more aggressive tumour phenotype (Fig. 1J, up, $P < 0.05$, Supporting Information Table S1). Kaplan−Meier analysis revealed that up-level expression of NFYB was associated with short disease-free survival of patients with HCC (Fig. 1K, $P < 0.01$, Supporting Information Table S2), which was consistent with the results in public TCGA datasets (Fig. S1C). Importantly, multivariate logistic regression analyses showed that highs level of NFYB were independent predictors for poor survival of patients with HCC ($P = 0.008$, Table S2).

Gene ontology analysis revealed that metastatic-specific accessible chromatin regions were associated with immune microenvironment, and we examined the CD45 expression in HCC samples by IF and IHC. Our results showed that CD45-positive immune cells were decreased in the TIME of HCC samples with the elevated level of NFYB (Fig. 1H−J). So NFYB may be associated with tumor immune microenvironment in HCC.

3.3. *NFYB promotes HCC progression and induces an inhibitory TIME*

We then explored the function of NFYB in HCC. NFYB was highly expressed in HCC cell lines, especially those with high

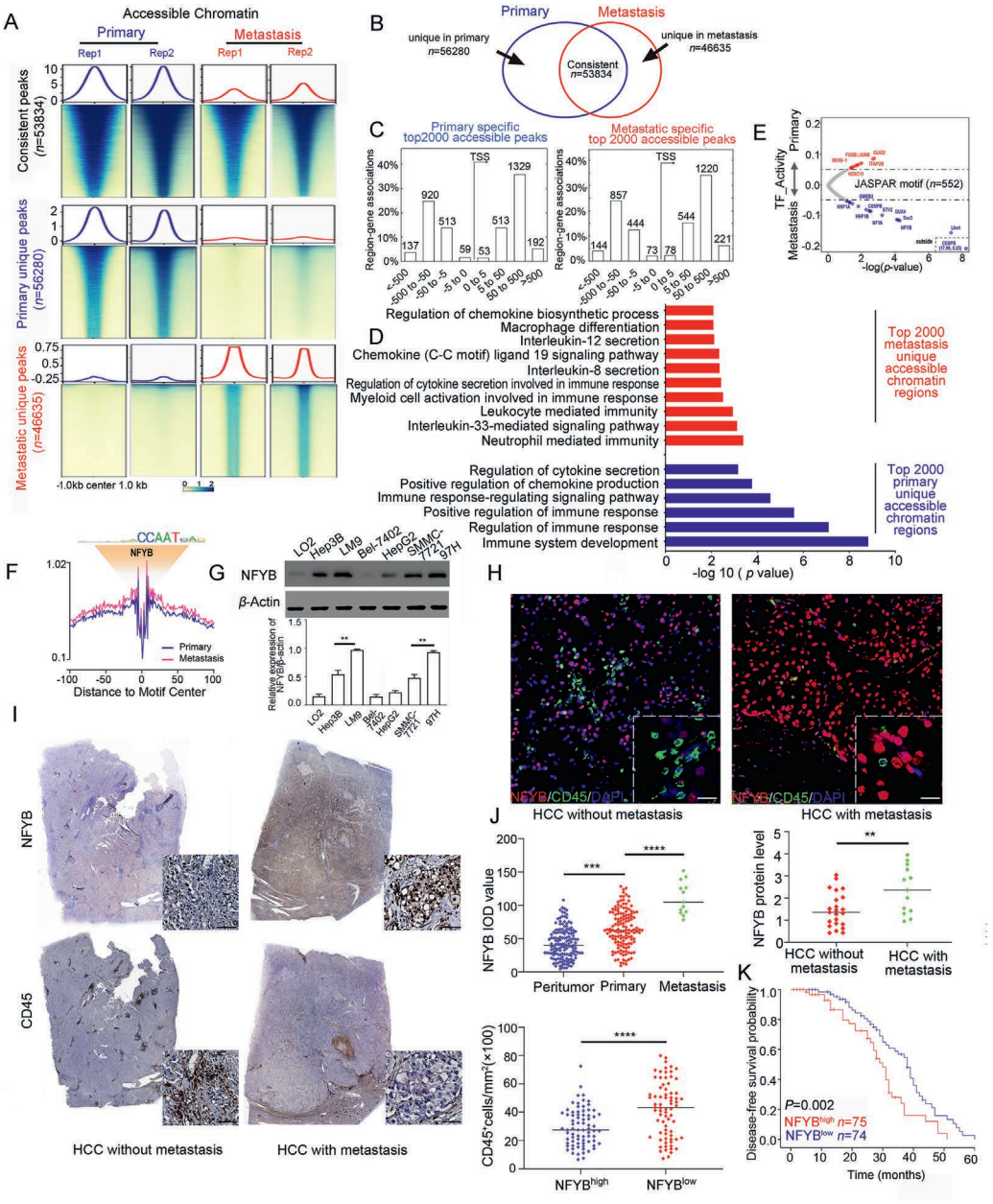

Figure 1 ATAC-seq analysis of two patient-derived primary/metastatic HCC pairs suggests that HCC may exist in at least two distinct chromatin accessibility states, with NFYB expression showing an apparent upregulation in metastatic HCC. (A) Density heat map of consistent-, loss- and gain-regions of accessible chromatin in primary and metastatic tumors. Motif enrichment was performed using Homer software. (B) Venn diagram showing the distribution of accessible chromatin regions in primary and metastatic tumors. (C) GREAT region-gene association graphs. Binned by orientation and distance to TSS. (D) GREAT gene ontology (GO) analysis of the top 2000 dynamic accessible chromatin regions. (E) Footprinting analyses for primary and metastatic tumors. (F) Downregulated chromatin accessibility of NFYB binding sites in primary and metastatic tumors. (G) Protein expression levels of NFYB in LO2 and six HCC cell lines. Down, the NFYB bands of the Western blot were analyzed using Image J. Data are the mean ± SD of three independent experiments, $n = 3$. $^{**}P < 0.01$. (H) Representative images of NFYB protein detection using IF assays. Red (NFYB + cells), green ($CD45^+$ cells). Scale bars, 50 μm. (I, J) IHC staining with NFYB-specific and CD45-specific antibodies to detect NFYB expression and $CD45^+$ lymphocyte infiltration in primary and metastatic tumours. Scale bars, 50 μm. (K) Kaplan−Meier analysis for survival of patients with HCC as a function of NFYB levels, $n = 149$, log-rank test, $P = 0.002$.

metastatic potential (Fig. 1G). We then generated the stable NFYB-knockout (single-guide NFYB) HCCLM9 and MHCC97H and NFYB-overexpressing HepG2 and Bel-7402 cell lines (Fig. S1D−S1G), and found that cell proliferation, motility, and invasion abilities were increased in $NFYB^{high}$ cells compared with those in $NFYB^{low}$ cells (Fig. 2A−D and Fig. S1H−S1K).

To determine whether NFYB regulates HCC metastasis in immunocompetent mice, Hepa1-6 cells which were infected with empty-lentivirus or NFYB-lentivirus (Fig. S1L and S1M) and C57BL/6 mice were used to establish the HCC xenograft. We collected the liver and lung tissues, and found that the NFYB-overexpressing group showed increased incidences of

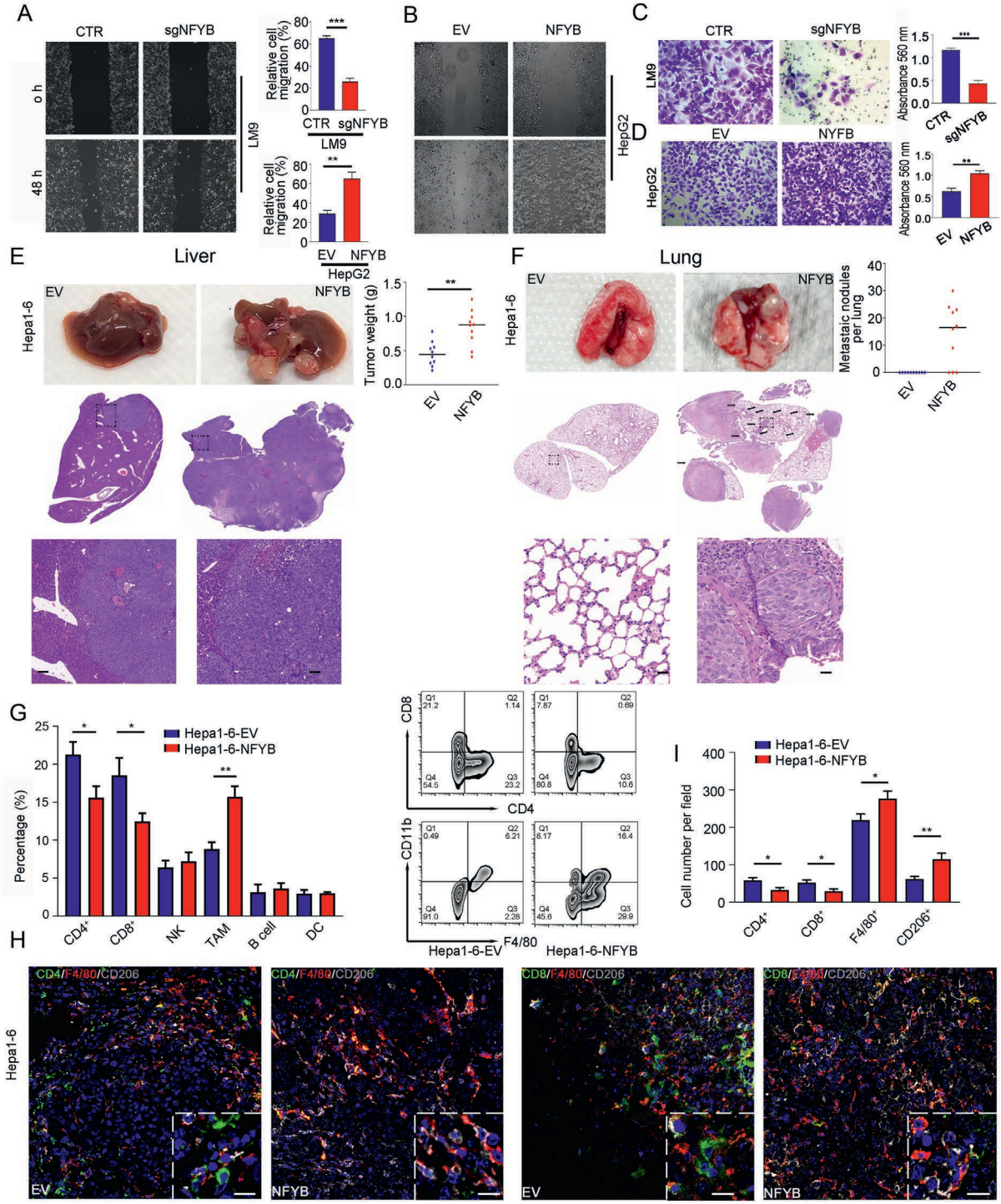

Figure 2 NFYB accelerates tumor progression and induces a suppressive TIME. (A, B) The wound-healing assay showed different motilities in control (Ctrl)-LM9, sgNFYB-LM9, empty vector (EV)-HepG2, and NFYB-HepG2 cell lines. The knockout of NFYB obviously inhibited the migration of LM9 lines (A). And the ectopic expression of NFYB significantly promoted the migration of HepG2 cell lines (B). Data are the mean ± SD of three independent experiments, $n = 3$. $^{*}P < 0.05$, $^{**}P < 0.01$, $^{***}P < 0.001$. (C, D) Cell invasion was evaluated using a Matrigel invasion chamber in control (CTR)-LM9, sgNFYB-LM9, empty vector (EV)-HepG2, and NFYB-HepG2 cell lines. The knockout of NFYB obviously inhibited the invasion of LM9 cell lines (C). And the ectopic expression of NFYB significantly promoted the invasion of HepG2 cell lines (D). Data are the mean ± SD of three independent experiments, $n = 3$. $^{*}P < 0.05$, $^{**}P < 0.01$, $^{***}P < 0.001$. Scale bar, 100 μm. (E, F) Representative photographs in livers (E) and lungs (F) were detected by H&E staining. Scale bars, 100 μm. (G) Tumour-infiltrating immune cells and inflammatory cells, including T cells ($CD4^+$ and $CD8^+$), natural killer (NK) cells (NK1.1+), B lymphocytes ($CD19^+$), DC cells (CD11c+) and TAMs (F4/80 + CD11b+) were detected by flow cytometry in liver tumour tissues. Right: representative flow cytometric analysis showing the proportion of $CD4^+$, $CD8^+$ T cells and TAMs in liver tumour tissues of mice. (H) Representative pictures of IF analysis in EV/NFYB mouses for CD4 (green), CD8 (green), F4/80 (red) and CD206 (grey) markers. Scale bar, 50 μm. (I) Quantification of corresponding immune cells by IF analysis. HCC, hepatocellular carcinoma; mIF, multiplex immunofluorescence; TIME, tumor immune microenvironment.

tumorigenesis, lung metastasis, larger tumor sizes and more tumor lesions relative to those in the EV group (Fig. 2E and F, Supporting Information Table S3). The percentage of tumour-infiltrating immune and inflammatory cells in mouse liver tumour tissues were assessed by flow cytometric analysis. We observed that TAMs were increased significantly, while $CD8^+$ and $CD4^+$ T cells were reduced in the NFYB-overexpressing group (Fig. 2G). Multiplex immunofluorescence assay confirmed the above results (Fig. 2H and I). Additionally, by employing a subcutaneous xenograft tumor model and further confirmed that $NFYB^{low}$ groups have lower tumor weights than $NFYB^{high}$ groups (Fig. S1N and S1O). These results indicate that NFYB promotes tumor progression and induces a suppressive TIME.

3.4. HCC-derived NFYB induces recruitment and M2-like polarization of macrophages

Since it has been known that immunosuppression may been powerfully induced by TAMs[23], we speculated that NFYB induced immunosuppression by promoting macrophage polarization and recruitment. Thus, we treated THP1 cells with phorbol-12-myristate-13-acetate (PMA) to differentiate them into macrophage (Supporting Information Fig. S2A). After being cocultured with $NFYB^{high}$ HCC cells, macrophages expressed high levels of CD163, CD206, p-STAT6 and PPARγ proteins, showed an upregulation of *CD206*, *IL-10*, *ARG1* and *PPAR*γ mRNA, and produced more IL-10 (Fig. 3A−C and Fig. S2B−S2F). Using a chemotactic migration assay, we found that $NFYB^{high}$ HCC cells promoted the chemotactic recruitment of macrophages (Fig. 3D and Fig. S2G). Phagocytosis assays also indicated that macrophages which were cocultured with $NFYB^{high}$ HCC cells displayed the lower phagocytic capacity (Fig. S2H). Moreover, macrophages cocultured with $NFYB^{high}$ HCC cells strongly suppressed T-cell proliferation and activation compared to those cocultured with $NFYB^{low}$ HCC cells (Fig. 3E and F, Fig. S2I and S2J). Together, these results suggest that NFYB-overexpressing HCC cells promote macrophage recruitment and M2-like polarization.

3.5. Deletion of TAMs suppresses NFYB-induced HCC metastasis

Next, we investigated the role of TAM in NFYB-induced HCC metastasis. Then we constructed the *Csf1*$^{op/op}$ mice that lack macrophages with mutated macrophage colony-stimulating factor 1 (*Csf1*) and then constructed orthotopic tumor xenograft models using Hepa1-6-NFYB cells. We found that deletion of TAM inhibited the NFYB-induced tumor growth and lung metastasis (Fig. 3G and H, Supporting Information Table S4). Flow cytometry and IF also confirmed that the $CD4^+$ and $CD8^+$ cells were significantly reduced in control mice, compared in *Csf1*$^{op/op}$ group (Fig. 3I−K). These results indicated that TAM contributed to NFYB-induced HCC metastasis.

3.6. LINC01137 inhibits NFYB degradation to promote macrophage polarization and recruitment

Many lncRNAs are involved in molecular signaling pathways through their interactions with proteins[19]. Feng et al.[24] reported that long non-coding RNA H19 recruits NFYB to activate MBTD1 and regulate doxorubicin resistance in lymphoma cells. Therefore, LM9 cells infected with lentivirus-HA-5′-NFYB/HA-3′-NFYB were immunoprecipitated with HA-antibody in order to diminish the non-specific interaction. And then HA pulldown showed a higher binding activity in LM9 cell with HA-5′-NFYB/HA-3′-NFYB, compared with control. Subsequently, this RNA immunoprecipitation was subjected to lncRNA microarray analysis. Analysis revealed 31 lncRNAs that co-associated with HA-3′ and HA-5′ (Fig. 4A), 11 lncRNAs of which were enriched with the HA-antibody in both HA-3′ and HA-5′ through RIP assay (Supporting Information Fig. S3A). However, LINC01137 was significantly upregulated in both NFYB-overexpressing LM9 cells and matched metastatic tumor tissues (Fig. S3B and S3C). Through 5′ and 3′ rapid amplification of cDNA ends, LINC01137 was characterized as a 1443 nucleotide (nt) transcript that is identical to NR_038842 (Genebank). Further, the association of NFYB with LINC01137 in LM9 cells was verified through RIP and RNA pulldown assays (Fig. 4B−D), which was also validated by the electrophoretic mobility shift assay (EMSA) (Fig. 4E). Furthermore, deletion-mapping analyses identified a 751−800 nt region of LINC01137 essential for its association with NFYB (Fig. 4F). Immunofluorescence and FISH revealed co-localization between NFYB and LINC01137 in LM9 and HCC97H cells (Fig. 4G and Fig. S3D), which were consolidated by the *in situ* hybridization for LINC01137 and immunohistochemistry for NFYB in HCC samples and the results from TCGA datasets (Fig. 4H and Fig. S3E and S3F). Subsequent analysis demonstrated the interaction of LINC01137 with NFYA and NFYC subunits (Fig. 4G, Fig. S3G and S3H). However, purified NFYA and NFYC proteins can't bind to LINC01137 full length (Fig. S3I), demonstrating the potential indirect binding of NFYA and NFYC to LINC01137 occurs *via* NFYB. To explore the functional relevance of the association of LINC01137 with NFYA, NFYB, and NFYC, LINC01137 knockdown was achieved in high metastatic cell lines (LM9 and 97H) which showed the highest LINC01137 levels (Fig. S3J and S3K and Supporting Information Fig. S4A). Despite a robust change in NFYB protein expression (Fig. 4I) and half-life (Fig. 4J), LINC01137 knockdown or overexpression did not impact the *NFYA*, *NFYC* mRNA and protein expression levels (Fig. S4B and S4C). In addition, LINC01137 knockdown-associated NFYB suppression was potentially rescued by the proteasome inhibitor, MG132 (Fig. 4K), indicating that LINC01137 protects NFYB from proteasome-dependent degradation. Furthermore, LINC01137 knockdown enhanced NFYB polyubiquitination (Fig. 4L). To investigate the mechanisms through which LINC01137 inhibits NFYB degradation, a series of NFYB mutants were generated to determine the binding motifs of LINC01137 with NFYB. The RNA pull-down assay showed that the NFYB mutant with 84−124 aa retained the capacity to associate with LINC01137 (Fig. S4D). Two candidate lysine sites in 84−124 aa were identified and substituted with alanine. Ubiquitination assays in WT or LNA1 LINC01137 LM9 cells displayed that the double K109/111A mutant blocked LINC01137LNA1 ubiquitination (Fig. 4M). Consistently, the RNA-pull down and RIP assays demonstrated that the K109/111A mutant blocked the association of LINC01137 with NFYB (Fig. 4N), and the abundance of the double mutant-enriched LINC01137 was greatly decreased compared to that of the wild-type and single mutant-enriched RNAs (Fig. 4O). Meanwhile, co-immunoprecipitation (Co-IP) and mass spectrometry were also conducted to identify the ubiquitin ligase TRIM25 which promoted the degradation of NFYB (Fig. S4E−S4I). Furthermore, the double K109/111A mutant also significantly inhibited the ubiquitination of the NFYB protein in TRIM25-overexpressing LM9 cells which were transfected with NFYB WT/mutant,

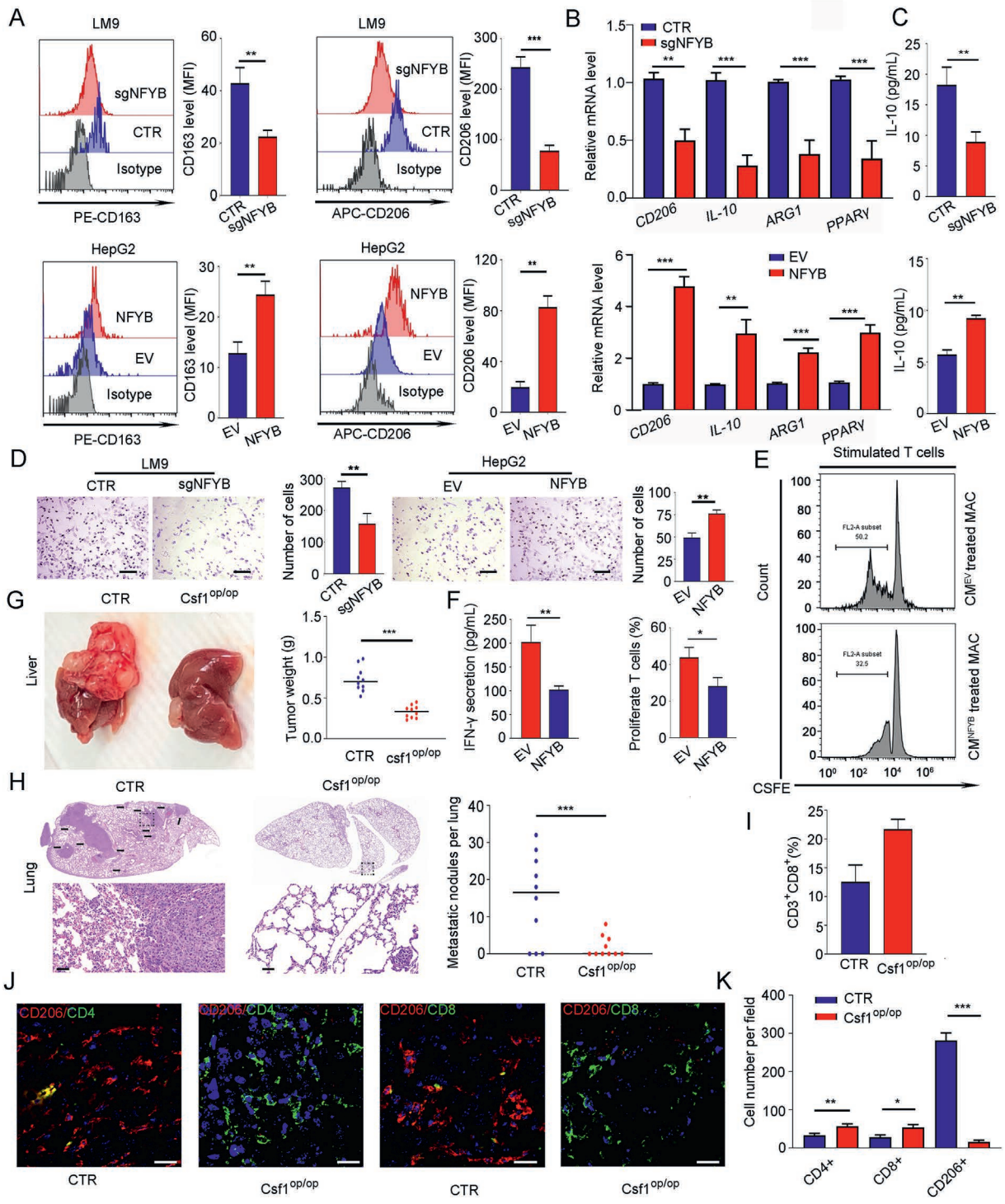

Figure 3 HCC-expressing NFYB induces recruitment and M2 polarization of macrophages and deletion of TAMs suppresses NFYB-induced HCC metastasis. (A) CD163 and CD206 expression in macrophages detected by FCM. FCM, flow cytometry. (B) *CD206*, *IL-10*, ARG1 and *PPARγ* mRNA levels in macrophages detected by qRT-PCR. qRT-PCR, quantitative reverse-transcription PCR. (C) Secreted IL-10 in the supernatants of macrophages detected by ELISA. (D) Chemotactic migration assays of macrophages using the supernatant of LM9-ctrl or -sgNFYB, HepG2-EV or -NFYB cells. Scale bar, 100 μm. (E) CFSE histograms detecting the promotion of T-cell proliferation by macrophages after treatment with the supernatant of HepG2-EV or -NFYB cells. MAC, macrophage. (F) IFN-γ secretion by $CD8^+$ T cells in the assay in (E), measured by ELISA. (G) Representative images of the liver in control (ctrl) and *Csf1*$^{op/op}$ orthotopic tumor xenograft models using Hepa1-6-NFYB cells mouse groups. Average tumor weight (Right) was determined. (H) Representative H&E staining of lung tissues (G) in HCC orthotopic xenograft ctrl or *Csf1*$^{op/op}$ models. The number of lung-colonizing nodules was calculated (Right). Scale bar, 100 μm. (I) Flow cytometric analysis $CD3^+CD8^+$ in tumours isolated from mice after orthotopic implantation. For down, mean ± SD, $n = 3$. $^*P < 0.05$, $^{**}P < 0.01$, $^{***}P < 0.001$ (unpaired t test). (J) IF staining images of $CD4^+$, $CD8^+$ T cells and TAM in tumours isolated from mice after orthotopic implantation. Scale bar, 25 μm. (K) Quantification of corresponding immune cells by IF analysis.

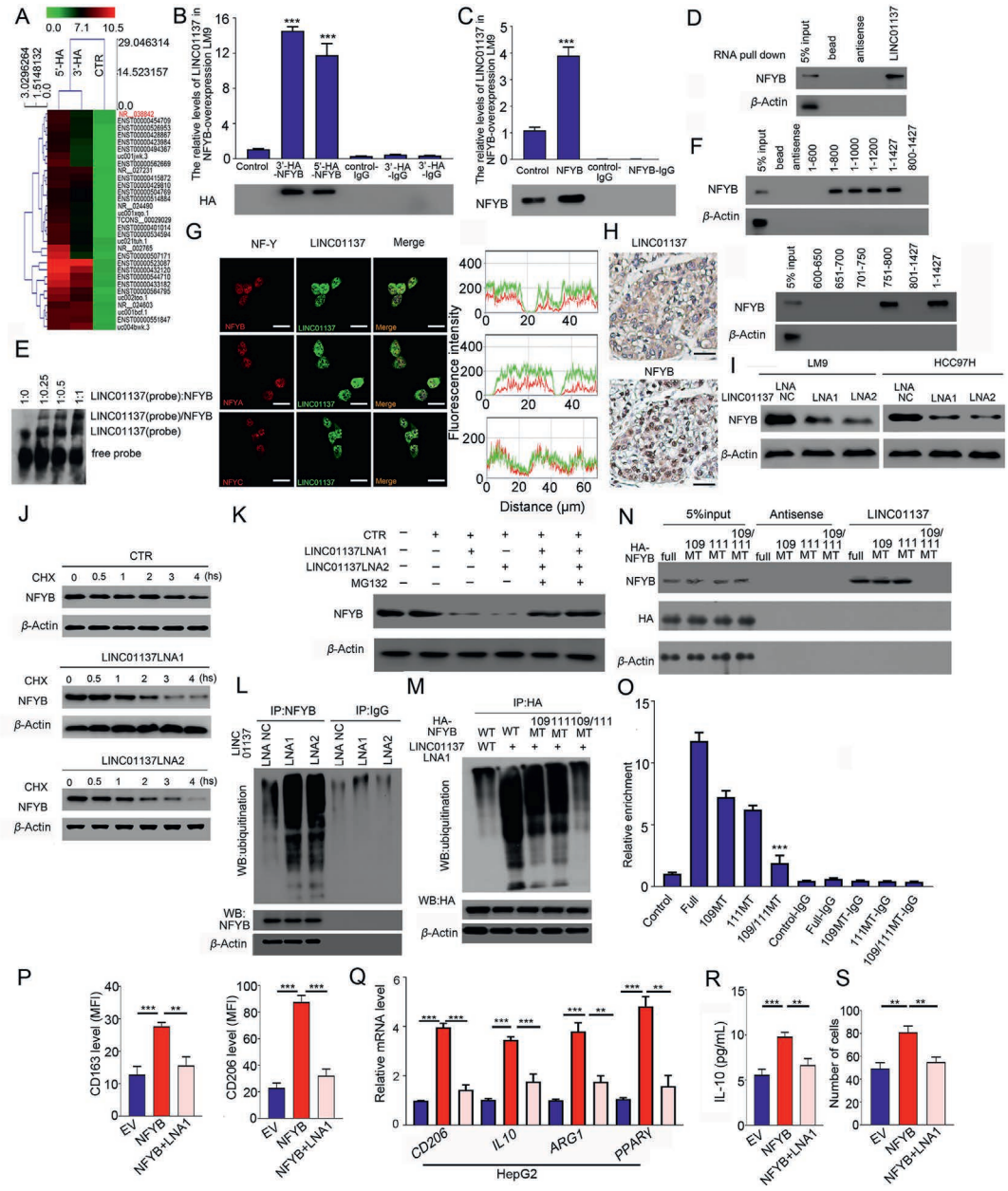

Figure 4 LINC01137 inhibits NFYB degradation in metastatic cell lines. (A) Hierarchical clustering analysis of lncRNAs recruited by HA in 3′-HA-NFYB and 5′-HA-NFYB-LM9 cells (greater than 2.0-fold; $P < 0.05$). Expression values above and below the median expression value across all samples are presented in red and green shades, respectively. (B, C) Recruitment of LINC01137 by anti-HA and anti-NFYB in HA-3′-NFYB-infected and HA-5′-NFYB-infected LM9 cells. (D) Western blot analysis of the specific association of NFYB with LINC01137 by RNA pull-down. (E) RNA EMSA demonstrating the binding capacity of NFYB to full-length LINC01137. LINC01137: NFYB indicates molar ratio. (F) RNAs corresponding to different fragments of LINC01137 or its antisense sequence were biotinylated and incubated with LM9 whole cell extracts ($n = 3$). (G) Co-localization of NFYA, NFYB, NFYC, and LINC01137 in LM9 cell lines, as determined by IF and FISH. Scale bar, 10 μm. Right: Fluorescence intensity profile. (H) Representative images of LINC01137 expression detected by ISH and NFYB expression detected by immunohistochemistry on adjacent consecutive sections. Scale bar, 50 μm. (I) Immunoblot assays of indicated proteins in LM9 and HCC97H cells which had been transfected with LNANC, LINC01137 LNA1 or LINC01137 LNA2 for 72 h. (J, K) LM9 cells which were transfected by LNANC, LINC01137LNA1 or LINC01137LNA2 were incubated with cycloheximide or in the presence or absence of MG132 (CHX, 0.5 μg/μL; MG132, 20 μmol/L) for the indicated time periods. Cell lysates were analyzed by Western blotting. (L) Cell lysates were immunoprecipitated with either control IgG or anti-NFYB antibody. Immunoprecipitates and input were analyzed by Western blotting. (M) LNANC or LINC01137LNA1 LM9 cells were transfected with HA-NFYB WT or mutant (K109A, K111A, and K109/111A) for 48 h, then cell lysates were immunoprecipitated with anti-HA antibody. (N, O) 293T cells expressing LINC01137 were transfected with pcDNA NFYB-HA-full or pcDNA NFYB-HA-mut (NFYB-HA-K109-mutant, NFYB-HA-K111-mutant, NFYB-HA-K109/K111-mutant) for 72 h, then cell lysates were prepared for RNA pulldown (N) and RNA immunoprecipitation (O) and qRT-PCR. RNA-pull down assay (N) displayed that the K109/111A mutant blocked the association of LINC01137 with NFYB. RIP assay (O) demonstrated that the abundance of the double mutant-enriched

LINC01137LNA1 (Fig. S4J). Furthermore, the ectopic expression of HA-NFYB mutant (K109A, K111A, and K109/111A) in LINC01137-LNA1LM9 cells significantly restored the migration and invasion (Fig. S4K and S4L). These results indicate that, by inhibiting 109/111 aa lysine ubiquitination, LINC01137 elevates NFYB protein levels *via* the ubiquitin-proteasome pathway by inhibiting 109/111 aa lysine ubiquitination.

Then, we investigated whether LINC01137 was the primary participant of NFYB-mediated processes. LINC01137 knockdown attenuated the levels of CD163 and CD206 (membrane protein), *CD206*, *ARG-1*, *IL-10* and *PPARγ* (mRNA), IL-10 (secreted proteins), the expression of p-STAT6 and PPARγ, and the chemotactic migration of macrophages induced by $NFYB^{high}$ HCC cells (Fig. 4P−S, Fig. S4M), and the phagocytic capacity and T-cell proliferation and activation were enhanced in cocultured macrophages by the transfection of LINC01137LNA1 (Fig. S4N−S4P). These results indicate that NFYB promotes macrophage recruitment and M2-like polarization largely through the fact that LINC01137 inhibits NFYB degradation.

3.7. Association of LINC01137 with SMYD3 and KAT2B

To further elucidate the molecular mechanisms through which LINC01137 regulates cytokine and chemokine expressions, the RNA pull-down assay was employed to screen for LINC01137-interacting proteins. Three independent RNA pull-down assays and RIP detection revealed that SMYD3 and KAT2B proteins were pulled down by LINC01137 (Fig. 5A and B, Supporting Information Fig. S5A and S5B, Table S5). Deletion mutants containing nt 100−150 and nt 1300−1350 interacted with SMYD3 and KAT2B, respectively (Fig. S5C and S5D). Next, two independent software programs (Mfold[25] and RNAfold[26]) were employed to predict the secondary structure of LINC01137 (nt 100−150, hA and 1300−1350, hB) (Fig. S5E and S5F), which was found to interact with SMYD3 and KAT2B in both RNA pull-down and EMSA assays, respectively (Fig. S5G and S5H).

We sought to establish the functional relevance of the correlation of LINC01137 with SMYD3/KAT2B. Notably, LINC01137 knockdown did not change the mRNA or protein expression levels of either SMYD3 or KAT2B in LM9 cells (Fig. S5I and S5J). Evidence indicates that SMYD3 and KAT2B are mainly localized in the nucleus[27,28]. Therefore, we performed nucleus fractionation which demonstrated the interaction of LINC01137 with SMYD3 and KAT2B in the nucleus (Fig. S5K). The co-IP assays performed in the nucleus of LM9 and HCC97H cells revealed that endogenous SMYD3 and KAT2B were specifically precipitated by anti-NFYB, NFYA, and NFYC antibodies (Fig. 5C, Fig. S5L and S5M). Thus, LINC01137 is associated with SMYD3 and KAT2B.

3.8. NF-Y expression in HCC regulates LINC01137 transcription

Surprisingly, the knockdown of NFYB in LM9 and 97H also decreased the LINC01137 levels (Fig. 5D). These observations prompted us to evaluate whether the NF-Y family regulates LINC01137 transcription.

To identify potential NFYB-binding sites at the LINC01137 promoter in HCC cell lines, we co-transfected a series of pGL3 reporter plasmids containing sequential deletions of the 5′-flanking regions upstream of LINC01137 and an NFYB-HA plasmid into HepG2 cell lines. The results revealed that deletion of the region from −1200 to −900 bp completely abrogated the luciferase activity (Fig. 5E). Sequence analysis showed the NFYB-binding site located at −936 to −921 bp upstream of the LINC01137 transcription start site. Nucleotide mutations at the NFYB-binding site were shown to significantly suppress luciferase activity (Fig. 5F). Furthermore, the binding of NFYB to its motif was verified through chromatin immunoprecipitation (ChIP) analysis using an anti-NFYB antibody (Fig. 5G).

3.9. NFYB is essential for the recruitment of KAT2B to the LINC01137 promoter

Co-IP analysis revealed that endogenic KAT2B potentially interacts with NFYB (Fig. 5C), and such association can be reinforced or inhibited by exogenous expression or knockdown of LINC01137, respectively (Fig. 5H and I). To elucidate the molecular mechanisms through which the NFYB/KAT2B protein complex is involved in the regulation of LINC01137 transcription, we co-transfected HepG2 cells with NFYB or/and KAT2B or NFYB/KAT2B/LINC01137 and a luciferase report construct. Individually compared with either NFYB or KAT2B, the Luc reporter was strongly activated by both NFYB/KAT2B (3.5-fold induction, Fig. 5J). Simultaneous transfections of NF-YB, KAT2B and LINC01137 further increased the promoter activity (6.7-fold induction, Fig. 5J). Moreover, A NFYB mutant lacking 53−142 aa, but known to contribute to subunit interactions and DNA binding, was used to evaluate the role of NF-YB in LINC01137 transcription[29]. Exogenous expression of the NFYB mutant impaired the contrasting transcriptional effects of NFYB/KAT2B/LINC01137 on LINC01137 promoter activity (Fig. 5J). As expected, ChIP analysis confirmed that KAT2B interactions with the LINC01137 promoter (Fig. 5K) can be abrogated by NFYB knockdown (Fig. 5L). This phenomenon was further demonstrated by downregulated LINC01137 levels in LM9 and HCC97H cells (Fig. 5M). Therefore, these findings indicate that KAT2B activates LINC01137 in an NFYB-dependent manner.

In vivo deletion of KAT2B and its family member (Gcn5) was shown to cause a dramatic reduction in H3K9 acetylation[30]. To elucidate the molecular mechanisms underlying KAT2B-dependent regulation of LINC01137, we evaluated the number of acetylated H3K9 (H3K9ac) associated with the LINC01137 promoter in LM9 and 97H cells. Notably, H3K9ac was recruited to the LINC01137 promoter (Fig. 5N). Furthermore, NFYB knockdown led to a significant reduction in H3K9ac (Fig. 5O), which was exacerbated by the simultaneous downregulation of NFYB and KAT2B and rescued by NFYB transfection in NFYB-knockdown cells (Fig. 5P and Q). These findings indicate that the

LINC01137 was greatly decreased compared to that of the wild-type and single mutant-enriched RNAs. (P) Quantification of CD163 and CD206 expression in macrophages using FCM analysis. (Q) *CD206*, *ARG1*, *IL-10* and *PPARγ* mRNA levels in macrophages, detected by qRT-PCR analyses. (R) Secreted IL-10 in macrophage supernatants, detected using ELISA. (S) Chemotactic migration assays of macrophages cocultured with HCC cells. For B, C, O, P, Q, R and S, P values were determined by two-sided unpaired t-test. Graphs show mean ± SD of experimental triplicates, $n = 3$. $^{*}P < 0.05$, $^{**}P < 0.01$, $^{***}P < 0.001$.

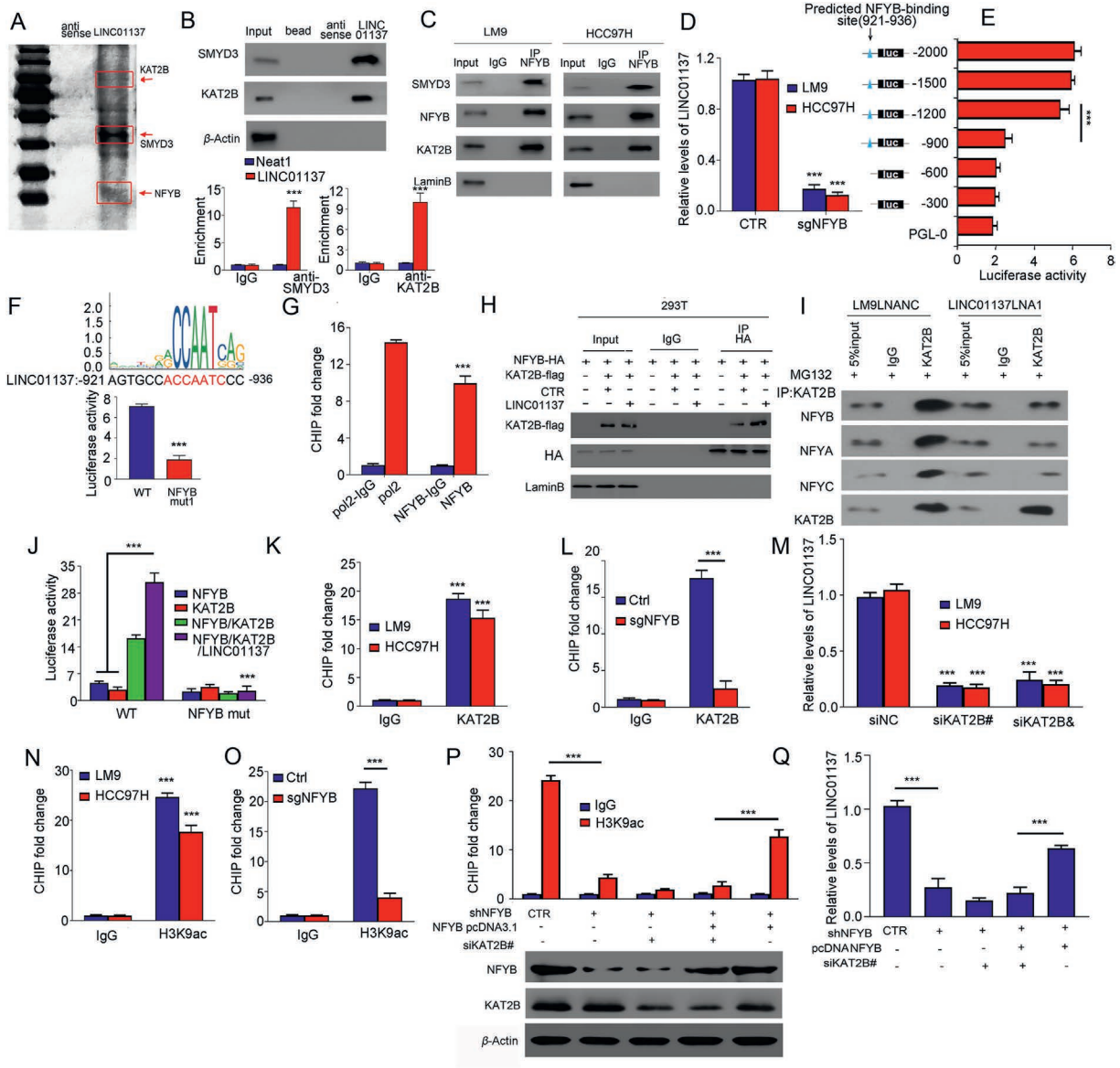

Figure 5 LINC01137 transcription is activated by a KAT2B/NFYB complex containing LINC01137 in a feed-forward loop. (A) LINC01137 interacts with both KAT2B and SMYD3, as detected by mass spectrum identifications. (B) LINC01137 binds to SMYD3 and KAT2B in nuclear extracts as shown by RNA-pulldown and RNA immunoprecipitation assay. (C) Immunoprecipitation analysis of interactions between endogenous NFYB and KAT2B, SMYD3 in LM9 and HCC97H cell nuclear extracts. (D) Relative mRNA levels of LINC01137 in LM9 cells with knockdown of NFYB. (E) Luciferase (luc) reporter assays for HepG2 cells co-transfected with reporter plasmids containing truncated LINC01137 promoters and NFYB-overexpressing vector for 48 h (wild type (WT), −2000 to +1 construct, −2000 to +1 construct with point mutation at the NFYB-binding site). (F) Luciferase (luc) reporter assays for HepG2 cells co-transfected with reporter plasmids containing wild-type (wt, up) or mutated (mut, down) LINC01137 promoters and NFYB-overexpressing vector for 48 h. (G) NFYB directly interacts with the LINC01137 promoter by ChIP assays. (H) Exogenous expression of LINC01137 increases the binding of NFYB to KAT2B. (I) LINC01137 knockdown reduces KAT2B binding to the NF-Y family. The transfected cells were treated with MG132 (20 μmol/L for 6 h) before being harvested. (J) HepG2 cells which were infected by CTR-lentivirus or LINC01137-lentivirus were co-transfected with pcDNA NFYB or/and KAT2B and luciferase report construct, containing wild-type and NFYB mutant without 53−142 amino acids for 48 h. (K) ChIP analysis for the localization of KAT2B at the LINC01137 promoter in LM9 and HCC97H cell lines. (L) Chromatin from control or NFYB-knockdown LM9 cells was immunoprecipitated with anti-KAT2B antibodies or normal IgG. (M) Relative mRNA levels of LINC01137 in KAT2B-knockdown LM9 cells. (N) ChIP analysis for the localization of H3K9ac at the LINC01137 promoter in LM9 and HCC97H cell lines. (O) Chromatin from control or NFYB-knockdown LM9 cells was immunoprecipitated with anti-H3K9ac antibodies or normal IgG. (P) ChIP-qPCR assays for CTR- or shNFYB-LM9 cells with or without siKAT2B or pcDNANFYB. (Q) Relative mRNA levels of LINC01137 in CTR- or shNFYB-LM9 cells with or without siKAT2B or pcDNANFYB. For A, D, G−N, *P* values were determined by two-sided unpaired *t*-tests. Graphs show mean ± SD of experimental triplicates, $n = 3$. $^{*}P < 0.05$, $^{**}P < 0.01$, $^{***}P < 0.001$.

KAT2B/NFYB complex activates LINC01137 transcription in a feed-forward loop.

3.10. LINC01137 promotes the formation of the SMYD3/NF-Y complex, thereby inducing the expression of IL-1β, CXCL2, and CCL20 via modulating active mark H3K4me3

To identify the factors of the promoting-tumor metastasis by LINC01137, RNA sequence analysis of LM9-LNANC and LM9-LINC01137LNA1 cells (Fig. S4A) was performed. After LINC01137 knockdown, approximately 120 genes were significantly downregulated by two-fold or more (Fig. 6A). The group of genes downregulated by LINC01137 knockdown was enriched in gene ontology annotations related to immune responses and cytokine(chemokine)-mediated signaling pathway (Supporting Information Fig. S6A), and associated genes were presented using a heatmap (Fig. 6B, Fig. S6B and S6C). Compared with LNA NC, LINC01137 knockdown significantly reduces mRNA and protein expression as well as the secretion of IL-1β, CXCL2, and CCL20 in LM9-LINC01137LNA1 cells (Fig. 6C and D). Furthermore, we investigated whether NFYB was the primary participant in the LINC01137/IL-1β/CXCL2/CCL20-mediated process. NFYB overexpression significantly increased mRNA and protein expression as well as the secretion of IL-1β, CXCL2, and CCL20 in HepG2 cells, which were also decreased by LINC01137 knockdown (Fig. 6E and F).

It has been demonstrated that SMYD3, which specifically methylates Lys-4 of histone H3[31,32] is an oncogenic driver that targets epigenetic regulation and signaling pathways[33]. Therefore, we co-transfected Hela cells with NFYB-HA, SMYD3-flag and control (CTR) or LINC01137. Subsequent IP assays showed that the addition of LINC01137 significantly enhanced the interaction of NFYB with SMYD3 (Fig. 6G), which was abolished by LINC01137 knockdown (Fig. 6H). Furthermore, ChIP assays showed that LINC01137 knockdown in LM9 cells reduced the occupancy of SMYD3 at the promoters of IL-1β, CXCL2, and CCL20 (Supporting Information Fig. S7A), which was further confirmed by ectopic transfection of LINC01137 LNA1 in NFYB-overexpressing-HepG2 cells (Fig. S7B). Moreover, the expression levels of IL-1β, CXCL2, and CCL20 were also significantly suppressed after LINC01137 and SMYD3 knockdown (Fig. S7C).

Studies have also reported elevated levels of the active mark H3K4me3 on the promoters of IL-1β, CXCL2, and CCL20 in neonatal monocytes, bone marrow neutrophils, and lymphatic metastasis[34-36]. Additionally, our studies observed that down-regulation of LINC01137 decreased H3K4me3 levels in both LM9 and 97H cell lines (Fig. 6I). ChIP−qPCR assays of LM9 cells demonstrated that H3K4me3 was laid down at the promoters of IL-1β, CXCL2, and CCL20 by LINC01137 knockdown (Fig. 6J). As anticipated, BCI-121, an inhibitor of H3K4me3 synthesis, suppressed the re-expression of *IL-1β*, *CXCL2*, and *CCL20* in LINC01137-overexpressing HepG2 cells (Fig. 6K). In addition, the overexpression of NFYB significantly increased H3K4me3 enrichment at the promoters of IL-1β, CXCL2, and CCL20, which was suppressed by knockdown of LINC01137 (Fig. 6L−N). Of note, this effect was intensified by the cooperative downregulation of LINC01137 and SMYD3 (Fig. 6L−N). To determine whether LINC01137 also regulates SMYD3 enzymatic activity *via* the NF-Y family, histone methyltransferase (HMT) assays were performed using LINC01137 and purified recombinant NFYB or SMYD3. Interestingly, *in vitro* addition of LINC01137 in NFYA/B/C and SMYD3 effectively increased HMT activity (Fig. 6O). These findings indicate that LINC01137 induces the expression of IL-1β, CXCL2, and CCL20 by promoting NFYB dependent recruitment of SMYD3 to modulate H3K4me3 levels.

3.11. The identified NFYB/LINC01137/IL-1β/CXCL2/CCL20 axis induces a suppressive TIME

According to these above results, we investigated whether IL-1β/CXCL2/CCL20 is a primary effector of NFYB/LINC01137-mediated processes. To determine the importance of IL-1β, CXCL2, and CCL20 in hepatocellular NFYB/LINC01137-mediated M2-like macrophage polarization, IL-1β, CXCL2, and CCL20 recombinant proteins were separately added into the conditional media of NFYB-overexpressing-HepG2 cells in which LINC01137 was simultaneously knocked down. The results showed that the recombinant protein fully restored the levels of CD206 and CD163 which were eventuated by the knockdown of LINC01137 (Fig. 7A). Notably, the addition of IL-1β neutralization antibody or knockdown of CXCL2 and CCL20 completely abolished macrophage polarization which was induced by the overexpression of LINC01137 (Fig. 7B).

To further determine the effects of NFYB/LINC01137/IL-1β/CXCL2/CCL20 on metastasis and M2-like macrophage polarization *in vivo*, Hep1-6 cells were first infected with lentivirus-CTR (CTR) and lentivirus-LINC01137. To confirm the critical role of CXCL2 and CCL20 in NFYB/LINC01137-mediated tumor metastasis, we knocked down CXCL2 and CCL20 in LINC01137-Hep1-6 cells. Then the above cells were injected into the tail veins of C57BL/6 immune-competent mice. *In vivo* treatment with the IL-1β inhibitor, diacerein (Dia) coupled with CCL20 and CXCL2 knockdown (Supporting Information Fig. S8A) suppressed tumor metastasis (Fig. 7C) and secretion of IL-1β, CCL20, and CXCL2 (Fig. S8B). Flow cytometry demonstrated that the abundance of both TAMs (Fig. 7D) and M-MDSCs (Fig. 7E) were decreased in Dia-treated Hepa1-6-LINC01137, Hepa1-6-LINC01137-shCCL20/CXCL2 tumors, while $CD3^+CD8^+$ T cells were increased (Fig. 7F). Furthermore, we found in humanized HCC lung metastatic mouse model that the tumour sizes (tumour weight) and the intrahepatic and pulmonary metastatic nodules were significantly decreased in the sgNFYB group compared with that in the CTR group ($P < 0.01$), and so were the percentages of TAM (Fig. S8C−S8E). Immunohistochemistry and *in situ* hybridization revealed that levels of LINC01137, IL-1β, CXCL2 and CCL20 were suppressed by the knockout of NFYB (Fig. S8F). Taken together, these findings suggest that NFYB/LINC01137/IL-1β/CCL20/CXCL2 signaling potentially promotes HCC metastasis by mediating TIME.

Clinically, we observed positive correlations between constituents of NFYB/LINC01137 axis and IL-1β/CXCL2/CCL20 in TCGA database (Fig. S8G). And in our HCC samples, we also found that high levels of NFYB, LINC01137, IL-1β, CXCL2, and CCL20 frequently occurred concomitantly (Fig. 7G and H), and the overactivated NFYB/LINC01137/IL-1β/CXCL2/CCL20 axis often induced an immunosuppressive microenvironment in HCC (Fig. 7I). These results indicate that the identified NFYB/LINC01137/IL-1β/CXCL2/CCL20 axis induces a suppressive TIME.

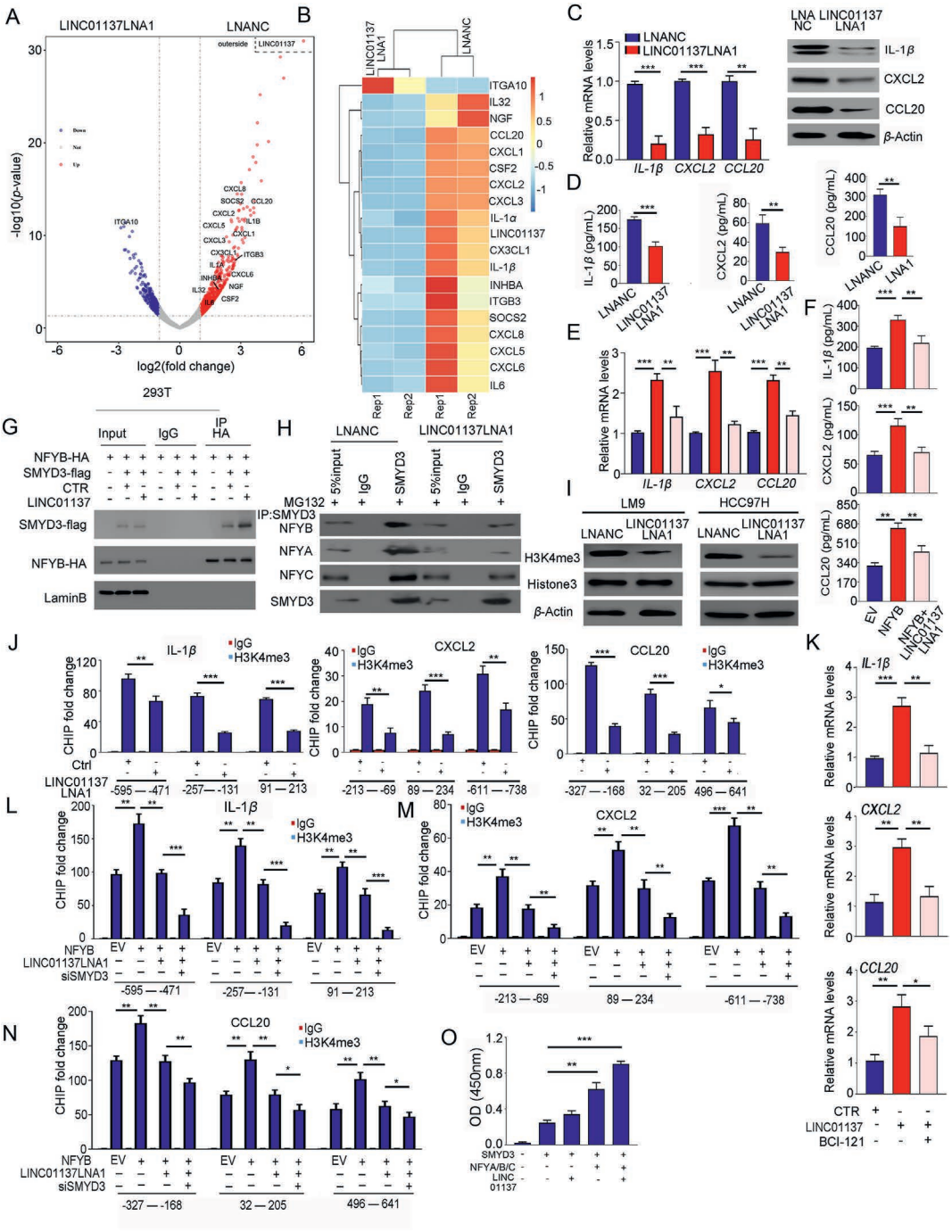

Figure 6 Ectopic expression of LINC01137 promotes M2 macrophage polarization and recruitment by upregulating IL-1β, CXCL2, and CCL20 secretion. (A) Differentially expressed genes in LM9-LNANC *versus* LM9-LINC01137 LNA1 cells. Blue and red dots represent differential RNA-seq expression decreased or increased by 2-fold or more (FDR<0.05), respectively, based on two independent biological replicates. (B) A heatmap showing differentially expressed genes that were correlated with immune responses. (C, D) mRNA and protein levels and secretion of IL-1β, CXCL2, and CCL20 in LM9-LNANC and LM9-LINC01137LNA1 cells. (E) IL-1β, CXCL1, and CCL20 mRNA levels in EV//NFYB/NFYB + LNA1-HepG2 cells. (F) Secreted IL-1β, CXCL1, and CCL20 in EV//NFYB/NFYB + LNA1-HepG2 cells. (G) Coimmunoprecipitation assay of interactions between exogenous NFYB and SMYD3. 293T cells infected with CTR-lentivirus or LINC01137-lentivirus were co-transfected with pcDNA NFYB-HA or/and SMYD3-flag for 72 h. Cell nuclear extracts were immunoprecipitated with HA antibody. (H) LM9 cells were transfected with LNANC or LINC01137LNA1 for 72 h, then the transfected cells were treated with MG132 (20 μmol/L for 6 h) before being harvested. Cell nuclear extracts were immunoprecipitated with IgG or SMYD3-antibody. (I) Immunoblot assays of indicated proteins in LNANC- and LINC01137LNA1-LM9/HCC97H cells. (J) ChIP-qPCR assays for HCC LM9 cells with LINC01137 knockdown. (K) IL-1β, CXCL2 and CCL20 mRNA expression levels in HepG2 cells with LINC01137 introduction exposed to BCI-121 (1 μmol/L) for 48 h. (L−N) ChIP-qPCR assays for empty (EV)- or NFYB-overexpressing-LM9 cells transfected with LINC01137LNA1 or/and siSMYD. (O) Histone methyltransferase assays. For C−F, J−O, *P* values were determined by two-sided unpaired *t*-test. Graphs show mean ± SD of experimental triplicates, $n = 3$. $^*P < 0.05$, $^{**}P < 0.01$, and $^{***}P < 0.001$.

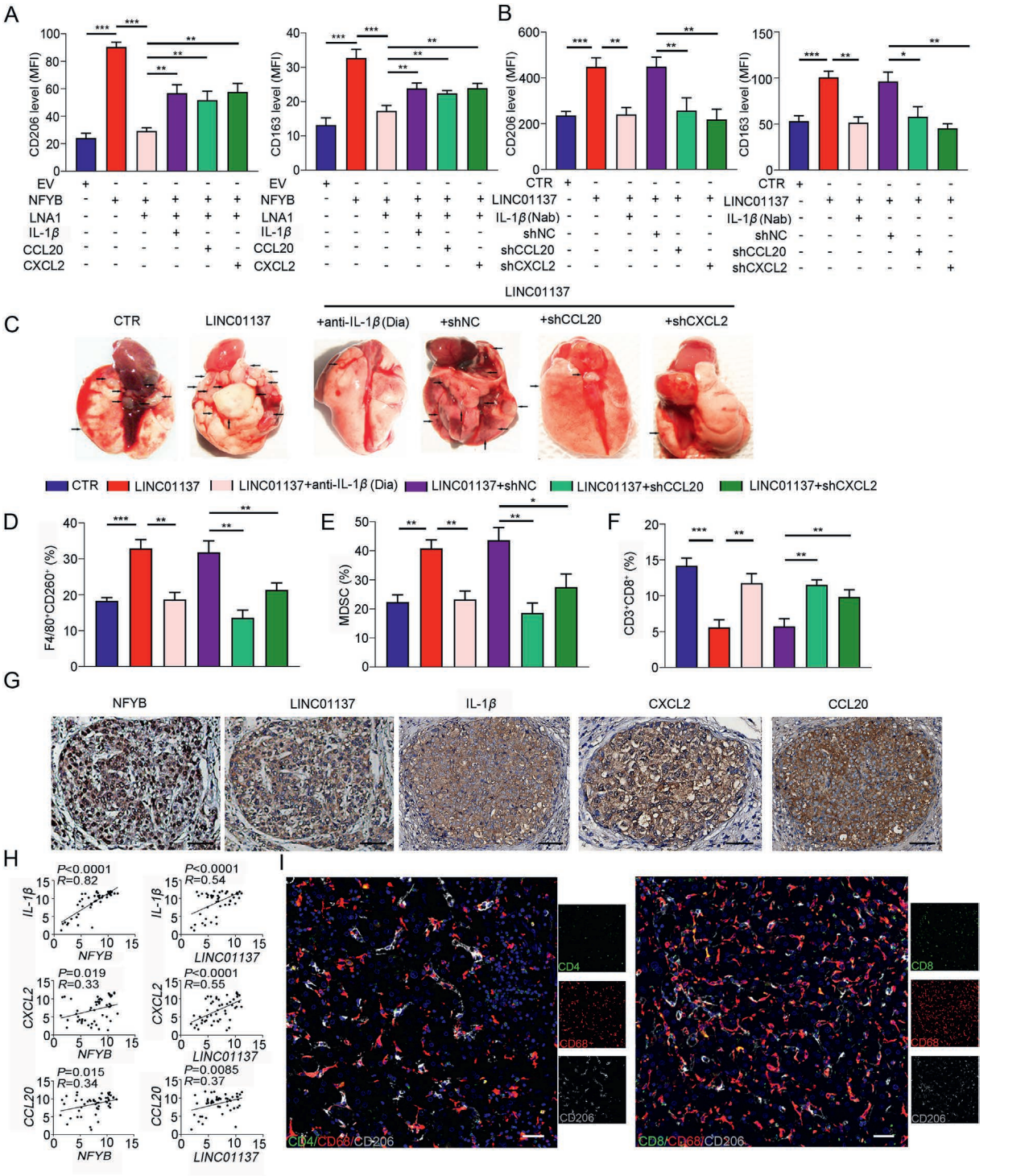

Figure 7 The identified NFYB/LINC01137/IL-1β/CXCL2/CCL20 axis induces a suppressive TIME. (A, B) Quantification of CD163 and CD206 expression in macrophages using FCM analysis. Recombinant IL-1β, CXCL2, and CCL20 protein (100 ng/mL), IL-1β neutralization antibody (Nab; 100 ng/mL). (C) Representative images showing the formation of tumor metastases in the mouse lung by each of the indicated Hepa1-6 populations. Arrows indicate metastatic tumors in the mouse lung. Mice were treated once a day by tail vein injection of IL-1β inhibitor diacerein (Dia, 20 mg/kg) (n = 5 mice per group). (D−F) Fractions of TAMs (B), MDSCs (C−E) and $CD3^+CD8^+$ T cells (F) in Hepa1-6-CTR/LINC01137 lung metastatic tumor were determined by flow cytometry as indicated in Fig. 7C (n = 5 mice per group). (G) Representative images of LINC01137 expression detected by ISH and NFYB, IL-1β, CXCL2, and CCL20 expression detected by immunohistochemistry. Scale bar, 20 μm. (H) Correlations among NFYB and LINC01137, IL-1β, CXCL2, and CCL20 in fifty HCC tumors and paired non-tumor tissues are denoted with Pearson's correlation coefficients (R). (I) Representative pictures of IF analysis in HCC samples for CD4 (green), CD8 (green), F4/80 (red) and CD206 (grey) markers. Scale bar, 25 μm.

3.12. The combination of anti-PD-L1 and IL-1β inhibitor Dia markedly inhibits NFYB-induced HCC metastasis

It has been reported that CXCL2 and CCL20 increased PD-L1 mRNA expression in lung adenocarcinoma and breast cancer[37,38]. And we examined PD-L1 expression in macrophages cocultured with NFYB-overexpressing HepG2 cells by flow cytometry. Surprisingly, levels of PD-L1 were significantly elevated in NFYB^{high} macrophages (Fig. 8A). In TCGA data, we also found that the expression of NFYB and LINC01137 was positively correlated with the one of PDL1 (Fig. S8G). And in order to investigate whether the combination of anti-PD-L1 with diacerein, which has been used to treat the inflammation-related diseases[39], has any effect on NFYB-mediated HCC metastasis, we constructed the orthotopic transplantation model with Hepa-1-6 cells overexpressing NFYB. Diacerein or anti-PD-L1 monotherapy partially reduced tumor growth and lung metastasis, whereas the combination therapy of both showed the strongest antimour effect (Fig. 8B−F). Meanwhile, the combination of anti-PD-L1 and diacerein observably augmented the percentage of $CD3^+CD8^+$ T cells and inhibited the TAM and MDSC accumulation (Fig. 8G and H). In conclusion, these results suggested that the combination of anti-PD-L1 and diacerein had significantly antitumour effects in NFYB-overexpressing HCC.

4. Discussion

Early metastasis seen in patients with HCC suggests that HCC has an inherent capacity to metastasize[40]. In the present study, we found that HCC tumors can gain metastatic potential through remodeling of chromatins (Fig. 8I). We used ATAC-seq to identify and analyze open chromatin regions that are specific to HCC metastasis. Moderate-to-high expression of NFYB was found in human HCC. And NFYB overexpression induces chromatin changes in human HCC. But ATAC-seq analysis relies on only two patient-derived primary/metastatic pairs, and this limited sample size raises concerns about generalizability given the heterogeneity of HCC. And these findings should be viewed as hypothesis-generating and warrant validation in larger cohorts.

How does NFY establish an open chromatin architecture? It has been demonstrated that the Histone-Fold domain protein, NF-Y, promotes chromatin accessibility by facilitating master/pioneer TF binding to enhancers or at distal regulatory regions[7,41]. Our results also indicated that the NF-Y family provides a strong footprinting signal in ATAC-seq data, a feature associated with slow DNA binding off-rate[42]. Furthermore, NF-Y binds to its consensus site with a high accuracy and fidelity, thereby alleviating the deleterious consequences of inaccurate transcription initiation and enforces a prototypical chromatin architecture with well-positioned nucleosomes[43,44]. These factors distinguish NFYB from other transcription factors. The present results indicate that NFYB establishes a pro-metastatic gene expression program by stabilizing chromatin accessibility at distal regulatory elements, a finding consistent with results from other studies. This suggests that the transcriptional role of NF-Y occurs at TSS-distal sites[41,45].

An implication of our study is that NFYB binds to nearby transcription factors and maintains an open chromatin architecture resulting in diverse functional outcomes. It has also been reported that NF-Y, which possess histone acetyltransferase activity by physically associating with other histone acetyltransferase enzymes[46], co-associates or co-localizes with a select cluster of growth-controlling and oncogenic TFs[45,47]. In this study, results showed that NFYB increased H3K4me3 levels at the promoters of IL-1β, CXCL2, and CCL20 by recruiting SMYD3. Moreover, it elevated H3K9ac levels at the promoter of LINC01137 by interacting with KAT2B, resulting in chemokine-mediated immunosuppressive microenvironments (Fig. 8I). These findings suggest that HCC uses NFYB-driven changes in chromatin state as a route for metastasis, although alternative pathways likely exist.

High expression of IL-1β, CXCL2, and CCL20 in the microenvironment of liver and other cancers triggers monocytes and macrophages recruitment into tumors to confer immune evasion[48-50]. The results showed that NFYB was upregulated in metastatic HCC cell lines, where it contributed to TAMs recruitment. RNA sequencing of LM9-LNANCand LM9-LINC01137LNA1 cells also revealed that a series of chemokines and cytokines are downregulated in LINC01137-kncokdown cells. In the *in vivo* metastatic model of HCC, treatment with the IL-1β inhibitor as well as CXCL2 and CCL20 knockdown significantly suppressed metastasis, partially by reducing immunosuppression in TAM and increasing the activity of cytotoxic $CD8^+$ T cells. These findings highlight that NFYB/LINC01137/SMYD3/IL-1β/CXCL2/CCL20 signaling axis often induces an immune-suppressive environment during HCC progression.

Evidence from preclinical and clinical studies suggests that TAMs are a major barrier to antitumor immunity in human HCCs[51,52]. As such, understanding the functions of TAM will inform the rational design of combination therapies[53,54]. In this study, it was found that the hepatocellular NFYB/LIN01137/SMYD3/IL-1β/CXCL2/CCL20 signaling axis mitigates antitumor T cell responses by inducing TAM immunosuppression. Clinically, concordant overexpression of NFYB is associated with more aggressive tumor phenotypes. Importantly, overexpression of NFYB was accompanied by high expression of PD-L1 in intratumoral tissues of HCC patients. Blocking IL-1β reduced immunosuppression, thereby rendering the tumor more susceptible to PD-L1 blockade[55]. Co-inhibition with IL-1β inhibitor and PD-L1 strengthened the $CD3^+CD8^+$ T cell responses and resulted in the complete remission of tumor-bearing mice. Treatment with an IL-1β inhibitor improved the efficacy of anti-PD-L1 therapy and altered the TIME *via* NFYB/LINC01137/IL-1β/CXCL2/CCL20 axis in HCC. Importantly, we presented extensive evidence that the combined treatment of diacerein with anti-PDL1 could synergistically improve the survival of tumor-bearing mice, especially in those with NFYB-overexpressing HCC.

It has been demonstrated that LINC01137 promotes tumor progression in oral squamous cell cancer and lung cancer[56,57]. And Tang et al.[58] reported that LINC01137 increased M2 macrophage mark by the modification of M2 macrophage orientation within the TIME in osteosarcoma, which is consistent with our results. Fan et al.[59] found that LINC01137 suppresses TGF-β-induced EMT and cancer cell plasticity. But our results displayed that the overexpression of LINC01137 increased the levels of TGF-β in cocultured macrophage cells. Maybe the high expression of LINC01137 produces a variety of cytokines and chemokines which results in the elevated levels of TGF-β.

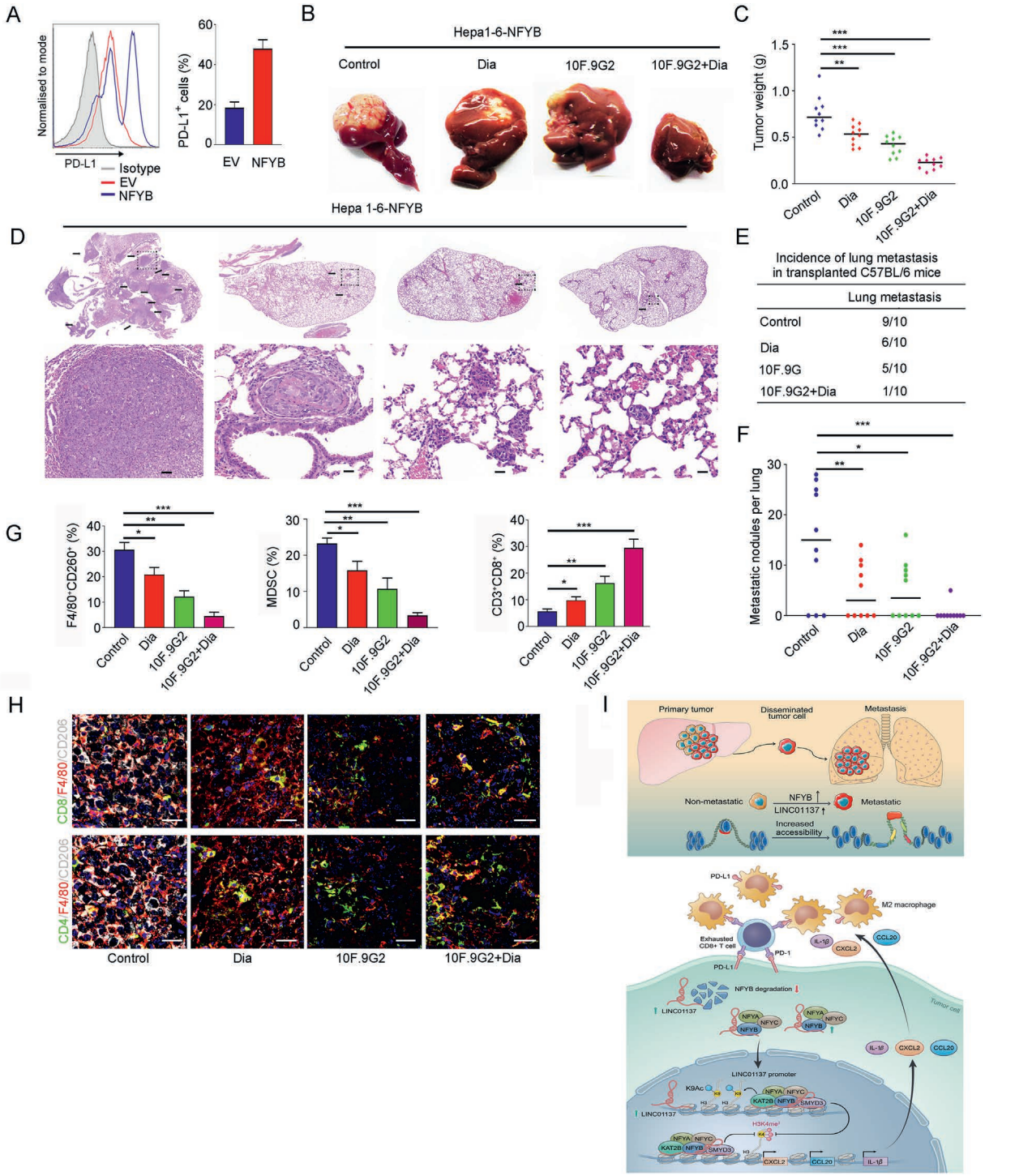

Figure 8 The combination of anti-PD-L1 and IL-1β inhibitor Dia markedly inhibits NFYB-induced HCC metastasis. (A) PD-L1 expression levels in macrophages cocultured with empty (EV) or NFYB-overexpressing HepG2 cells by flow cytometry. *P* values were determined by two-sided unpaired *t*-test. Graphs show mean ± SD of experimental triplicates, $n = 3$. $^{*}P < 0.05$, $^{**}P < 0.01$, $^{***}P < 0.001$. (B) Representative image of the liver in HCC orthotopic xenograft ($n = 10$ mice/group). (C) Average tumor weight (Right) was determined. (D) Representative H&E staining of lung tissues in HCC orthotopic xenograft models. Scale bar, 100 μm. (E) Incidence of lung colonization was calculated. (F) The number of lung-colonizing nodules was calculated. (G, H) Flow cytometric analysis and IF staining images of $CD8^{+}$ T cells, TAM, and MDSC in tumours isolated from mice after orthotopic implantation. For down, mean ± SD, $n \geq 3$. $^{*}P < 0.05$, $^{**}P < 0.01$, $^{***}P < 0.001$ (unpaired *t* test). Scale bar, 25 μm. (I) model showing NFYB/LINC01137/IL-1β/CXCL2/CCL20-axis-regulated metastatic progression. HCC metastases exhibit profound chromatin changes compared to primary tumors. NFYB increases chromatin accessibility at distal regulatory elements. LINC01137 mitigates antitumor T cell responses by promoting M2 macrophages polarization. This is accomplished by stabilizing NFYB to recruit SMYD3, which in turn upregulates IL-1β, CXCL2, and CCL20. The NFYB/KAT2B complex activates LINC01137 transcription through a feed-forward loop.

5. Conclusions

We determined that the NFYB−lncRNA axis favors an inhibitory TIME by promoting M2-like polarization in recruited macrophages, and diacerein reshapes the tumor microenvironment and reverses anti-PDL1 susceptibility. Our study reveals a promising therapeutic regimen for combination therapy with anti-PDL1.

Acknowledgements

This study was supported by grants from the Natural Science Foundation of China (81772613, 81774378, 82272638, and 82003253). Jiangxi Province 'Ganpo Talent Program' Innovation Leadership Talent (gpyc20240199, China). Natural Science Foundation of Jiangxi Province (20242BAB20404, 20252BAC240624, China). Science and Technology Plan Project of Jiangxi Provincial Health Commission (202610030, China). Key Project of Jiangxi Provincial Department of Education (GJJ2400104, China). The First Affiliated Hospital of Nanchang University Young Talent Research Cultivation Fund (YFYPY2023103, China). Science and Technology Plan Project of Jiangxi Provincial Administration of Traditional Chinese Medicine (2024A0090, China). The Full Time Talent Introduction and Research Start up Fund of the First Affiliated Hospital of Nanchang University (RSC-0020, China). J.C. acknowledges the Fundação Ciência e Tecnologia, IP national support, through CHRC (04923/2020) and the FCT Grant LISBOA2030-FEDER-00862500-14998.

Author contributions

Fang Zheng, João Conde and Zifeng Wang conceived the ideas and designed the experiments. Boxuan Zhou, Qiang Tao, Wu Wen, Jianan Tan, Jie Xu, Yixuan Fang, and Xiaorong Lin performed the experiments. Zifeng Wang and Jie Xu provided the patient samples for clinical data analysis. Jiao Guan, Milad Ashrafizadeh, João Conde and Jiehua He analyzed the data. Fang Zheng and João Conde wrote the paper.

Ethics statement

This study was approved by the ethics committee of the First Affiliated Hospital, Jiangxi Medical College, Nanchang University (Nanchang, China) [Ethics approval number: (2024) CDYFYYLK (05-008)]. All animal experiments were approved by the animal ethics committee of the First Affiliated Hospital, Jiangxi Medical College, Nanchang University (Animal ethics approval number: CDYFY-IACUC-202407QR174).

Conflicts of interest

João Conde is a co-founder and shareholder of TargTex S.A.—Targeted therapeutics for Glioblastoma Multiforme. João Conde is a member of the Global Burden Disease (GBD) consortium of the Institute for Health Metrics and Evaluation (IHME), University of Washington (US) and is on the Scientific Advisory board of Vector Bioscience Cambridge. The other authors have no conflicts of interest to declare.

Data and material availability

The microarray and ATAC-seq/RNA-seq data referenced during the study are available in a public repository from the website https://www.ncbi.nlm.nih.gov/geo/query/acc.cgi?acc=GSE154509 (GSE154509) and http://bigd.big.ac.cn/gsa/s/4x06IRy (CRA002814).

Appendix A. Supporting information

Supporting information to this article can be found online at https://doi.org/10.1016/j.apsb.2026.03.037.

References

1. Toh MR, Wong EYT, Wong SH, Ng AWT, Loo LH, Chow PK, et al. Global epidemiology and genetics of hepatocellular carcinoma. *Gastroenterology* 2023;**164**:766−82.
2. Llovet JM, Montal R, Sia D, Finn RS. Molecular therapies and precision medicine for hepatocellular carcinoma. *Nat Rev Clin Oncol* 2018;**15**:599−616.
3. Wei CY, Zhu MX, Zhang PF, Huang XY, Wan JK, Yao XZ, et al. PKCalpha/ZFP64/CSF1 axis resets the tumor microenvironment and fuels anti-PD1 resistance in hepatocellular carcinoma. *J Hepatol* 2022;**77**:163−76.
4. Xie M, Lin Z, Ji X, Luo X, Zhang Z, Sun M, et al. FGF19/FGFR4-mediated elevation of ETV4 facilitates hepatocellular carcinoma metastasis by upregulating PD-L1 and CCL2. *J Hepatol* 2023;**79**:109−25.
5. Mantovani R. The molecular biology of the CCAAT-binding factor NF-Y. *Gene* 1999;**239**:15−27.
6. Nardini M, Gnesutta N, Donati G, Gatta R, Forni C, Fossati A, et al. Sequence-specific transcription factor NF-Y displays histone-like DNA binding and H2B-like ubiquitination. *Cell* 2013;**152**:132−43.
7. Oldfield AJ, Yang P, Conway AE, Cinghu S, Freudenberg JM, Yellaboina S, et al. Histone-fold domain protein NF-Y promotes chromatin accessibility for cell type-specific master transcription factors. *Mol Cell* 2014;**55**:708−22.
8. Gatta R, Mantovani R. NF-Y affects histone acetylation and H2A.Z deposition in cell cycle promoters. *Epigenetics* 2011;**6**:526−34.
9. Gurtner A, Fuschi P, Magi F, Colussi C, Gaetano C, Dobbelstein M, et al. NF-Y dependent epigenetic modifications discriminate between proliferating and postmitotic tissue. *PLoS One* 2008;**3**:e2047.
10. Gurtner A, Manni I, Piaggio G. NF-Y in cancer: impact on cell transformation of a gene essential for proliferation. *Biochim Biophys Acta Gene Regul Mech* 2017;**1860**:604−16.
11. Zhang Y, Huang H, Liu P, Xie Y. NFYB increases chemosensitivity in glioblastoma by promoting HDAC5-mediated transcriptional inhibition of SHMT2. *J Neuropathol Exp Neurol* 2023;**82**:911−20.
12. Feng L, Xu X, Zhao K. NFYB potentiates STK33 activation to promote cisplatin resistance in diffuse large B-cell lymphoma. *Leuk Res* 2021;**111**:106708.
13. Tharyan RG, Annibal A, Schiffer I, Laboy R, Atanassov I, Weber AL, et al. NFYB-1 regulates mitochondrial function and longevity *via* lysosomal prosaposin. *Nat Metab* 2020;**2**:387−96.
14. Lu T, Li C, Xiang C, Gong Y, Peng W, Hou F, et al. Over-expression of NFYB affects stromal cells reprogramming and predicts worse survival in gastric cancer patients. *Aging* 2022;**14**:7851−65.
15. Bezzecchi E, Ronzio M, Mantovani R, Dolfini D. NF-Y overexpression in liver hepatocellular carcinoma (HCC). *Int J Mol Sci* 2020;**21**:9157.
16. Wang H, Ma Z, Xu M, Xiong M, Chen X, Zhou Y, et al. Coptisine-mediated downregulation of E2F7 induces G2/M phase arrest in hepatocellular carcinoma cells through inhibition of E2F4/NFYA/NFYB transcription factors. *Chem Biol Interact* 2024;**397**:111063.
17. Guttman M, Rinn JL. Modular regulatory principles of large non-coding RNAs. *Nature* 2012;**482**:339−46.

18. Kopp F, Mendell JT. Functional classification and experimental dissection of long noncoding RNAs. *Cell* 2018;**172**:393−407.
19. Tang L, Li G, Chang J, Xian H, Liu Y, Lin L, et al. Elevated SNHG15 empowers keratinocytes hyperproliferation through activation of STAT3/Cyclin D1 axis in psoriasis. *Acta Pharm Sin B* 2025;**15**:6430−43.
20. Feretzaki M, Pospisilova M, Valador Fernandes R, Lunardi T, Krejci L, Lingner J. RAD51-dependent recruitment of TERRA lncRNA to telomeres through R-loops. *Nature* 2020;**587**:303−8.
21. Love MI, Huber W, Anders S. Moderated estimation of fold change and dispersion for RNA-seq data with DESeq2. *Genome Biol* 2014;**15**:550.
22. Li Z, Schulz MH, Look T, Begemann M, Zenke M, Costa IG. Identification of transcription factor binding sites using ATAC-seq. *Genome Biol* 2019;**20**:45.
23. Kloosterman DJ, Akkari L. Macrophages at the interface of the co-evolving cancer ecosystem. *Cell* 2023;**186**:1627−51.
24. Feng L, Yan Q, Xu X. Long non-coding RNA H19 recruits NFYB to Aactivate MBTD1 and regulate doxorubicin resistance in lymphoma cells. *Mol Biotechnol* 2023;**65**:997−1009.
25. Zuker M. Mfold web server for nucleic acid folding and hybridization prediction. *Nucleic Acids Res* 2003;**31**:3406−15.
26. Hofacker IL. Vienna RNA secondary structure server. *Nucleic Acids Res* 2003;**31**:3429−31.
27. Ishikura S, Nakabayashi K, Nagai M, Tsunoda T, Shirasawa S. ZFAT binds to centromeres to control noncoding RNA transcription through the KAT2B−H4K8ac−BRD4 axis. *Nucleic Acids Res* 2020;**48**:10848−66.
28. Sarris ME, Moulos P, Haroniti A, Giakountis A, Talianidis I. Smyd3 is a transcriptional potentiator of multiple cancer-promoting genes and required for liver and colon cancer development. *Cancer Cell* 2016;**29**: 354−66.
29. Sinha S, Kim IS, Sohn KY, de Crombrugghe B, Maity SN. Three classes of mutations in the A subunit of the CCAAT-binding factor CBF delineate functional domains involved in the three-step assembly of the CBF−DNA complex. *Mol Cell Biol* 1996;**16**:328−37.
30. Jin Q, Yu LR, Wang L, Zhang Z, Kasper LH, Lee JE, et al. Distinct roles of GCN5/PCAF-mediated H3K9ac and CBP/p300-mediated H3K18/27ac in nuclear receptor transactivation. *EMBO J* 2011;**30**:249−62.
31. Hamamoto R, Furukawa Y, Morita M, Iimura Y, Silva FP, Li M, et al. SMYD3 encodes a histone methyltransferase involved in the proliferation of cancer cells. *Nat Cell Biol* 2004;**6**:731−40.
32. Van Aller GS, Reynoird N, Barbash O, Huddleston M, Liu S, Zmoos AF, et al. Smyd3 regulates cancer cell phenotypes and catalyzes histone H4 lysine 5 methylation. *Epigenetics* 2012;**7**:340−3.
33. Bottino C, Peserico A, Simone C, Caretti G. SMYD3: an oncogenic driver targeting epigenetic regulation and signaling pathways. *Cancers (Basel)* 2020;**12**:142.
34. Bermick JR, Lambrecht NJ, denDekker AD, Kunkel SL, Lukacs NW, Hogaboam CM, et al. Neonatal monocytes exhibit a unique histone modification landscape. *Clin Epigenet* 2016;**8**:99.
35. Nguyen-Jackson HT, Li HS, Zhang H, Ohashi E, Watowich SS. G-CSF-activated STAT3 enhances production of the chemokine MIP-2 in bone marrow neutrophils. *J Leukoc Biol* 2012;**92**:1215−25.
36. Huang M, Dong W, Xie R, Wu J, Su Q, Li W, et al. HSF1 facilitates the multistep process of lymphatic metastasis in bladder cancer *via* a novel PRMT5-WDR5-dependent transcriptional program. *Cancer Commun* 2022;**42**:447−70.
37. Inoue C, Miki Y, Saito R, Hata S, Abe J, Sato I, et al. PD-L1 induction by cancer-associated fibroblast-derived factors in lung adenocarcinoma cells. *Cancers (Basel)* 2019;**11**:1257.
38. Kwantwi LB, Wang S, Zhang W, Peng W, Cai Z, Sheng Y, et al. Tumor-associated neutrophils activated by tumor-derived CCL20 (C−C motif chemokine ligand 20) promote T cell immunosuppression *via* programmed death-ligand 1 (PD-L1) in breast cancer. *Bioengineered* 2021;**12**:6996−7006.
39. Sun L, Huang X, Wang J, Yuan C, Zhao H, Li D, et al. Eltrombopag plus diacerein *vs* eltrombopag in patients with ITP: a multicenter, randomized, open-label phase 2 trial. *Blood* 2024;**144**:1791−9.
40. Banales JM, Inarrairaegui M, Arbelaiz A, Milkiewicz P, Muntane J, Munoz-Bellvis L, et al. Serum metabolites as diagnostic biomarkers for cholangiocarcinoma, hepatocellular carcinoma, and primary sclerosing cholangitis. *Hepatology* 2019;**70**:547−62.
41. Arampatzi P, Gialitakis M, Makatounakis T, Papamatheakis J. Gene-specific factors determine mitotic expression and bookmarking *via* alternate regulatory elements. *Nucleic Acids Res* 2013;**41**:2202−15.
42. Sung MH, Guertin MJ, Baek S, Hager GL. DNase footprint signatures are dictated by factor dynamics and DNA sequence. *Mol Cell* 2014;**56**: 275−85.
43. Li J, Shen S, Chen J, Liu W, Li X, Zhu Q, et al. Accurate annotation of accessible chromatin in mouse and human primordial germ cells. *Cell Res* 2018;**28**:1077−89.
44. Oldfield AJ, Henriques T, Kumar D, Burkholder AB, Cinghu S, Paulet D, et al. NF-Y controls fidelity of transcription initiation at gene promoters through maintenance of the nucleosome-depleted region. *Nat Commun* 2019;**10**:3072.
45. Fleming JD, Pavesi G, Benatti P, Imbriano C, Mantovani R, Struhl K. NF-Y coassociates with FOS at promoters, enhancers, repetitive elements, and inactive chromatin regions, and is stereo-positioned with growth-controlling transcription factors. *Genome Res* 2013;**23**:1195−209.
46. Currie RA. NF-Y is associated with the histone acetyltransferases GCN5 and P/CAF. *J Biol Chem* 1998;**273**:1430−4.
47. Myers JA, Couch T, Murphy Z, Malik J, Getman M, Steiner LA. The histone methyltransferase Setd8 alters the chromatin landscape and regulates the expression of key transcription factors during erythroid differentiation. *Epigenetics Chromatin* 2020;**13**:16.
48. Karki R, Kanneganti TD. Diverging inflammasome signals in tumorigenesis and potential targeting. *Nat Rev Cancer* 2019;**19**:197−214.
49. Lin H, Yan J, Wang Z, Hua F, Yu J, Sun W, et al. Loss of immunity-supported senescence enhances susceptibility to hepatocellular carcinogenesis and progression in toll-like receptor 2-deficient mice. *Hepatology* 2013;**57**:171−82.
50. Wei Y, Lao XM, Xiao X, Wang XY, Wu ZJ, Zeng QH, et al. Plasma cell polarization to the immunoglobulin G phenotype in hepatocellular carcinomas involves epigenetic alterations and promotes hepatoma progression in mice. *Gastroenterology* 2019;**156**:1890−904.
51. Liu M, Zhou J, Liu X, Feng Y, Yang W, Wu F, et al. Targeting monocyte-intrinsic enhancer reprogramming improves immunotherapy efficacy in hepatocellular carcinoma. *Gut* 2020;**69**:365−79.
52. Wang D, Li X, Li J, Lu Y, Zhao S, Tang X, et al. APOBEC3B interaction with PRC2 modulates microenvironment to promote HCC progression. *Gut* 2019;**68**:1846−57.
53. Liu X, Zhang Q, Liang Y, Xiong S, Cai Y, Cao J, et al. Nanoparticles (NPs)-mediated Siglec15 silencing and macrophage repolarization for enhanced cancer immunotherapy. *Acta Pharm Sin B* 2023;**13**: 5048−59.
54. Wang F, You H, Liu H, Qi Z, Shi X, Jin Z, et al. Silencing PTPN2 with nanoparticle-delivered small interfering RNA remodels tumor microenvironment to sensitize immunotherapy in hepatocellular carcinoma. *Acta Pharm Sin B* 2025;**15**:2915−29.
55. Kaplanov I, Carmi Y, Kornetsky R, Shemesh A, Shurin GV, Shurin MR, et al. Blocking IL-1beta reverses the immunosuppression in mouse breast cancer and synergizes with anti-PD-1 for tumor abrogation. *Proc Natl Acad Sci U S A* 2019;**116**:1361−9.
56. Du Y, Yang H, Li Y, Guo W, Zhang Y, Shen H, et al. Long non-coding RNA LINC01137 contributes to oral squamous cell carcinoma development and is negatively regulated by miR-22-3p. *Cell Oncol* 2021;**44**:595−609.
57. Yao Y, Yang F, Chen A, Hua Q, Gao W. Costimulatory molecule-related lncRNA model as a potential prognostic biomarker in non-small cell lung cancer. *Cancer Med* 2023;**12**:6419−36.
58. Tang N, Chen Y, Su Y, Zhang S, Huang T. The role of disulfidptosis-associated LncRNA-LINC01137 in osteosarcoma biology and its regulatory effects on macrophage polarization. *Funct Integr Genomics* 2024; **24**:219.
59. Fan C, Wang Q, Kuipers TB, Cats D, Iyengar PV, Hagenaars SC, et al. LncRNA LITATS1 suppresses TGF-beta-induced EMT and cancer cell plasticity by potentiating TbetaRI degradation. *EMBO J* 2023;**42**: e112806.